# Water-Vapor Responsive and Erasable Metallo-Peptide Nanofibers

Avishek Dey*,[1] Elma Naranjo,[1,2] Ranajit Saha,[3] Sheng Zhang,[1] Maya Narayanan Nair,[1] Tai-De Li,[1] Xi Chen*,[1,2,4,6] Rein V. Ulijn*[1,5,6,7]

**ABSTRACT:** Short peptides are versatile molecules for the construction of supramolecular materials. Most reported peptide materials are hydrophobic, stiff, and show limited response to environmental conditions in the solid-state. Herein, we describe a design strategy for minimalistic supramolecular metallo-peptide nanofibers that, depending on their sequence, change stiffness, or reversibly assemble in the solid-state, in response to changes in relative humidity (RH). We tested a series of histidine (H) containing dipeptides with varying hydrophobicity, XH, where X is G, A, L, Y (glycine, alanine, leucine, and tyrosine). The one-dimensional fiber formation is supported by metal coordination and dynamic H-bonds. Solvent conditions were identified where GH/Zn and AH/Zn formed gels that upon air-drying gave rise to nanofibers. Upon exposure of the nanofiber networks to increasing RH, a reduction in stiffness was observed with GH/Zn fibers reversibly (dis-)assembled at 60-70 % RH driven by a rebalancing of H-bonding interactions between peptides and water. When these metallo-peptide nanofibers were deposited on the surface of polyimide films and exposed to varying RH, peptide/water-vapor interactions in the solid-state mechanically transferred to the polymer film, leading to the rapid and reversible folding-unfolding of the films, thus demonstrating RH-responsive actuation.

Supramolecular materials based on biological building blocks hold promise for various applications in biotechnology, materials science, and medicine.[1-7] Water is often the solvent of choice, driving self-assembly of sequence-specific biopolymers to form structures with wide-ranging properties. Peptide and protein-based materials are increasingly considered for applications outside aqueous environments, including the solid-state, *e.g.* as electronic wires, films, surface coatings, actuators, or barrier materials.[8-13] For these solid-state applications, peptide nanostructures are typically assembled in aqueous media and then dried.[14-17] Their dynamics, integrity, or functionality may be compromised in the absence of liquid water and the hydrophobic effect.

Peptide- and protein-based materials that retain their structures in the dried state are typically stiff fibrous materials, such as silks, elastin-like peptides, and amyloid structures with hydrophobic domains rich in strongly directional H-bonding patterns.[18-21] Other examples used in the solid-state are minimalistic hydrophobic peptides (such as diphenylalanine, FF, or the related proline tripeptide, (PFF), peptide amphiphiles that are functionalized with aromatic residues.[22-26] These materials can be remarkably stable in the solid-state [27-29], and some of them can also be assembled in non-aqueous media.[30-32] Both the formation conditions of supramolecular fibers and their solid-state stability and responsiveness requires consideration of solvent interactions.[33-36] There are currently few examples of peptide or protein-based materials that display stimuli-responsiveness in the solid-state, yet such materials hold promise as actuators and tunable barriers.[37]

Herein, we introduce a design approach for polar peptide nanofibers that are stable under dry conditions and responsive to water-vapor in the solid-state. We opted for a strategy that combines metal coordination and H-bonding interactions to support fiber formation through a combination of His-Zn coordination observed in metalloproteins, amyloid fibers, and peptide-based materials,[38-45] thereby de-emphasizing the role of aromatic amino acids in a hydrophobic core,[46,47] complemented by flexible H-bonding domains to favor competing interactions with water-vapor (Figure 1).

The designs were inspired by metallo-peptide-based porous materials that undergo conformational change in the presence of guest solvents or gas molecules.[38,39] A recent report shows that reversible metal/peptide coordination can lead to changes in amphiphilicity, conformation, and stabilization of emulsions.[41] We selected four histidyl dipeptides, combining His-Zn coordination and varying polarity at the N-terminal (Log P: -3.11 (GH)> -2.62 (AH)> -1.39 (LH)>-1.34 (YH)) (Figure 1A). To find conditions for self-assembly of Zn(II)/dipeptides to form nanofiber networks, we considered water and water/methanol mixtures with varying pH to influence solubility and the protonation state of imidazole and termini (Figure 1B and Table S1-S3). All four peptides were fully soluble in water at 10 mM. In MeOH, AH and LH precipitated, while GH and YH remained soluble. In 1:9 water/MeOH mixtures at acidic pH (2-3), clear solutions were obtained both in the absence or presence of $ZnCl_2$ due to protonation of the imidazole nitrogen, preventing binding to Zn (II).[41,45] At pH~12, it was found that GH and AH formed gels in presence of $ZnCl_2$. Deprotonation of carboxylic acid was deemed essential for metal coordination and consequent gelation (Figure 1B). LH/Zn and YH/Zn precipitated under these conditions. These results demonstrate that tuning the hydrophobicity of the N-terminal amino acid (G <A <L <Y) and nonaqueous solvation at elevated pH impacts on the metallo-peptide assembly. It was also noticed that the gelation of GH/Zn (12h) occurred much faster compared to the AH/Zn (48h) (Figure S1 and Table S3). The mechanical strength of the GH/Zn and AH/Zn gels were assessed by oscillatory rheology, demonstrating viscoelastic properties (Figure S2).

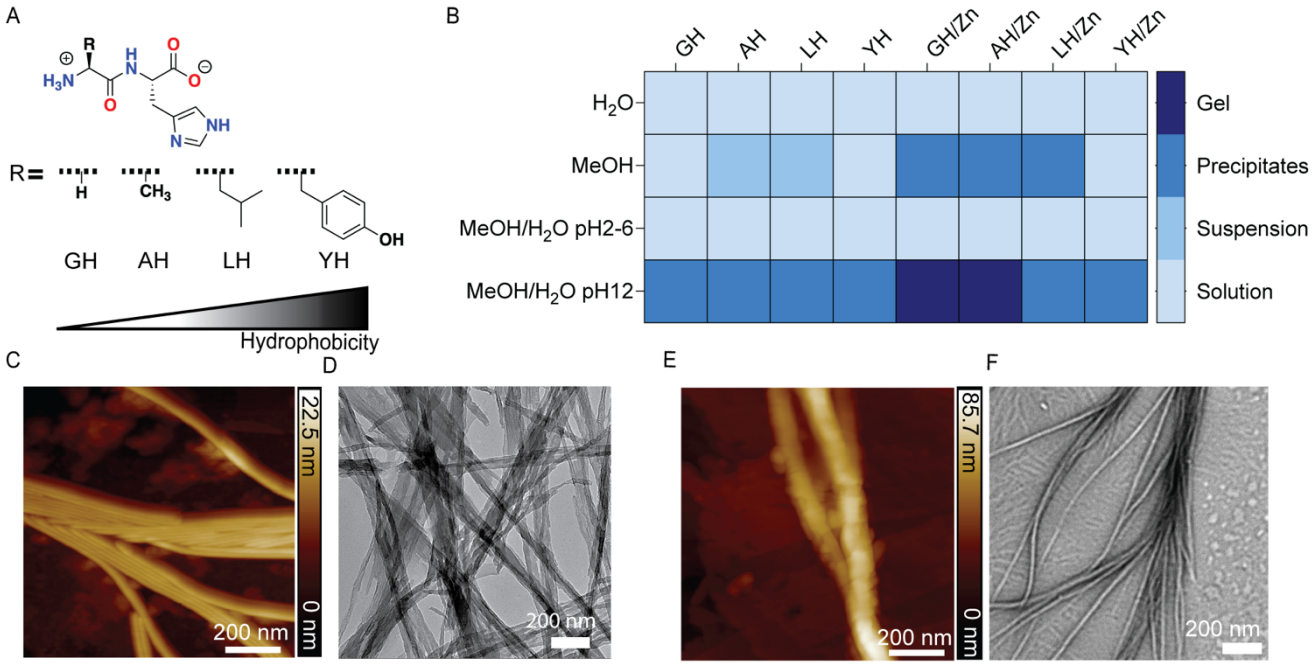


**Figure 1.** (A) Metallo-dipeptide design with varying hydrophobicity. (B) Exploration of solvent conditions in presence of 10 mM dipeptides with and without 10 mM Zn(II). (C-F) AFM and TEM images indicating the formation of the twisted nanofibers structures of **GH/Zn** (C and D) and **AH/Zn** (E and F) post solvent evaporation.

To measure the stability of the nanofibers in the dry state, the gels were deposited on a silicon wafer and carbon grid, air dried for 24h and analyzed using atomic force microscopy (AFM) and transmission electron microscopy (TEM). AFM revealed nanofibers for GH/Zn (Figure 1C and Figure S3) and AH/Zn (Figure 1E and Figure S4) (with the former having a chiral appearance), and amorphous aggregates for LH/Zn and YH/Zn (Figure S5). The twisted appearance of nanofibers assembled from GH/Zn compared to the AH/Zn may be related to the flexible backbone for GH (Figures S3-S4). TEM analysis also confirmed the formation of nanofibers for both the GH/Zn (Figure 1D and Figure S3) and AH/Zn (Figure 1F and Figure S4).

To gain supramolecular structural insights in the dry state, several complementary spectroscopic techniques were employed. We performed solid-state $^{13}C$ cross-polarization magic angle spinning (CP-MAS) NMR experiments on the air-dried samples of GH/Zn, AH/Zn, GH, and AH dipeptides. $^{13}C$ CP-MAS NMR shows the characteristic peak shifting and broadening of carbonyl carbon (-C=O) at 174 and 177 ppm for GH and GH/Zn carboxylate (-COO) due to Zn-O bonding interactions (Figure 2A).[44,48] The broadening of the amide (-CONH-) carbonyl (-C=O) (164 ppm) peak suggests the presence of hydrogen bonding interactions between the amide carbonyl groups. The peak at 134 and 127 ppm of GH was downfield shifted to 142 and 136 ppm indicating coordination of the imidazole nitrogen with Zn (II).[8,48] The glycine -$CH_2$ peak also downfield shifted from 40 to 45 ppm from GH to GH/Zn, confirming side chain interactions, in line with previous observations for Zn-coordinated peptide structures.[38,39] The peak at the beta $CH_2$ also downfield shifted from 28 to 30 ppm from GH to GH/Zn. CP-MAS NMR supported the assemblies of GH/AH and Zn (II) with respect to coordination and side chain interactions (Figure 2B for AH/Zn and Figure S6-S9).

X-ray photoelectron spectroscopy (XPS) analysis further confirmed the metallo-peptide coordination for GH/Zn and AH/Zn. Deconvolution for GH/Zn of O1s spectrum exhibited peaks at 529.79 eV indicating the Zn-O bond.[49,50] The additional peak at 532.84 eV corresponds to water/MeOH and 528.20 eV indicated C=O bonds (Figure 2C). Deconvolution of the Zn2p3/2 spectra revealed that the presence of Zn-N (1018.75 eV) and Zn-O bond (1019.84 eV) (Figure 2D). Deconvolution of the N1s spectrum exhibited peak at 397.39 eV which indicates the Zn-N bond. Further, C1s spectra supported the presence of peptide associated C=O, C-O, C-N, C-C, C-H bonding interactions (Figure S10). Similarly, XPS of AH/Zn also suggested the formation of the metallo-peptide nanofibers through metal-peptide binding. Deconvolution of O1s spectra indicating the Zn-O bond and C=O bonds, Zn2p3/2 spectra revealed that the presence of Zn-N and Zn-O bond for AH/Zn (Figure 2E, 2F and Figure S11).

Self-assembled nanofibers were further analyzed by Raman spectroscopy, showing changes in molecular interaction of the GH upon Zn (II) coordination.[51-52] The metal-peptide coordination and dynamic H- bonds caused Raman peak shifts compared with those of its metal-free dipeptide (Figure S12). The hydrogen bonding was verified with Fourier transform infrared spectroscopy (FT-IR) with an intense peak at 3100-3400 $cm^{-1}$ which indicates potential presence of hydrogen bonding. The signal at 1623 $cm^{-1}$ indicates C=O and His stretching and the signal at 1455 $cm^{-1}$ also indicates carboxylate symmetric stretching for metal binding (Figure S13 and S14). Based on the above evidences, we propose the supramolecular architecture shown in Figure 2G where $COO^-$ and imidazole coordinate with Zn(II) to form $Zn(GH)_2$/ $Zn(AH)_2$. We note that a similar tetrahedral coordination arrangement was found to be favored in Aß-Zn(II) metalloprotein complexes, albeit with $COO^-$ ligand provided by Glu/Asp side chains.[47]

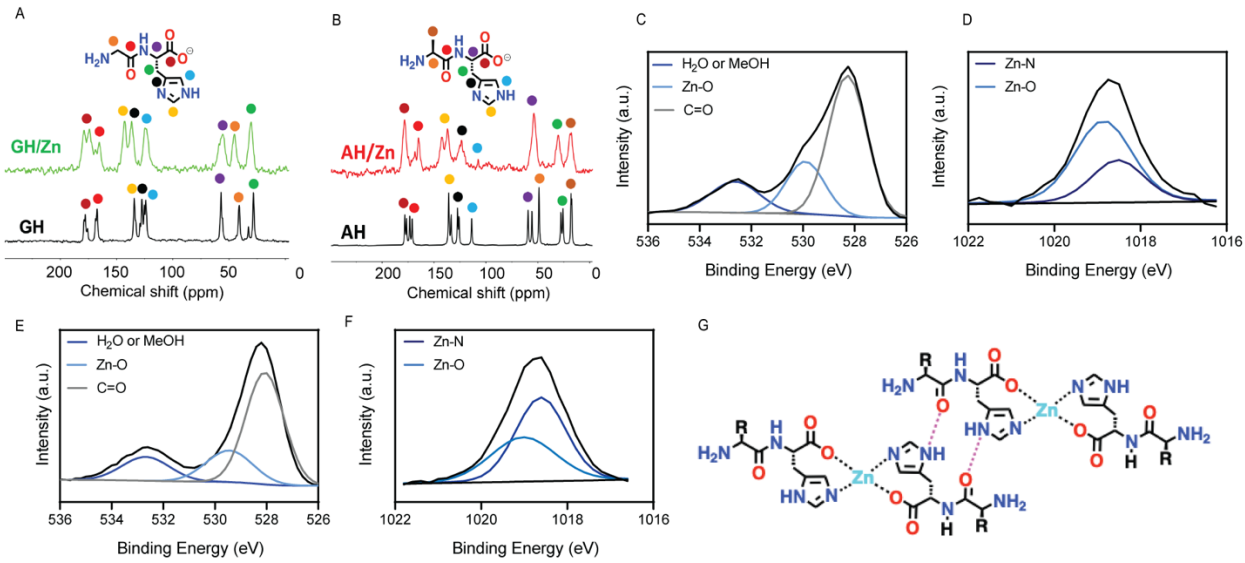


**Figure 2.** Structural characterization of metallo-peptide nanofibers of **GH/Zn** and **AH/Zn** upon air-drying from the gel state. $^{13}C$ Solid-state CPMAS NMR spectra of the GH and GH/Zn (A), and AH and AH/Zn nanofibers (B) showing chemical shift changes upon nanofiber formation in the dry state upon Zn(II) coordination. (C-F) XPS analysis confirmed the binding between metal and peptide in the GH/Zn and AH/Zn xerogel in the dry state. Deconvolution of the O1s spectrum revealed peaks at 529.79 eV indicating the presence of Zn-O bonds (C) and Zn2p3/2 spectra showed the presence of Zn-N (1018.75 eV) and Zn-O bonds (1019.84 eV) for GH/Zn (D), whereas deconvolution of O1s spectrum revealed peaks at 529.4 eV indicating the presence of Zn-O bonds (E) and Zn2p3/2 spectra showed the presence of Zn-N (1018.6 eV) and Zn-O bonds (1019.3 eV) (F) for AH/Zn. (G) Proposed core structure of metallo-peptide nanofibers.

To further verify the feasibility of these structures, geometry optimizations at RI-B3LYP-D3(BJ)/def2-SVP were performed to estimate the metal-peptide interactions (Figure 3 and details in SI computation part). Density functional theory (DFT) suggested the feasibility of the proposed Zn-O and Zn-N binding modes for the monomers of the GH/Zn and AH/Zn (Figure 3A, 3E and Figure S30 in SI), respectively. The noncovalent interactions plots depict the stabilization of the side chains over the His for GH/Zn (Figure 3B, 3C and Figure S31,32 in SI) and AH/Zn (Figure 3F, 3G and Figure S31,32 in SI). The proposed monomer structure also suggests the feasibility of the one-dimensional assembly *via* directional hydrogen bonding between the imidazole of His and amide C=O groups, with polar groups presented at the fiber surface, and a core that is stabilized by Zn(II) coordination (Figure 3D and Figure 3H). The formation of the dimers is found to be favorable process (Figure 3B, 3F and Figure S33 in SI). The calculated dimerization energy ($\Delta E_d$) and enthalpy of dimer formation ($\Delta H_d$) are -18.2 and -12.4 kcal/mol and -16.8 and -10.8 kcal/mol, respectively (SI, Table S4), proving the more likelihood of GH/Zn to form head-on association and one-dimensional fiber formation compared to that of AH/Zn. The NCI plots of $(GH/Zn)_2$ (Figure 3C) and $(AH/Zn)_2$ (Figure 3G) clearly exhibit blue colored surfaces, indicating the C=O···H–N hydrogen bonds in both cases. The origin of the C=O···H–N hydrogen bonds in $(GH/Zn)_2$ can be demonstrated from comparing Figure S32 and S33 in SI. In case of the decamers, the average C=O···H–N hydrogen bonds distances are 1.677 Å and 1.702 Å for GH/Zn and AH/Zn, respectively. The adaptability in the GH/Zn (Figure 3D) drives the chiral/twisted appearance of the nanofibers compared to the AH/Zn (Figure 3H). The stability lies in the noncovalent interactions present therein as shown in Figure S34 in SI. The overall architecture generates polar fibers with a metallo-coordinated core (Figure 2G).

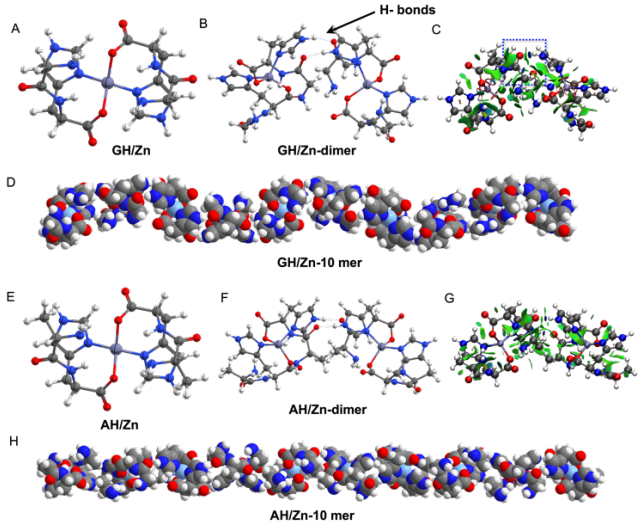


**Figure 3.** Illustrations of the DFT optimized structure. (A, E) Coordination unit of **GH/Zn** (top) and **AH/Zn** (bottom). (B, F) Energy minimized dimer of **GH/Zn** (top) and **AH/Zn** (bottom) shows strongly directional hydrogen bonding between imidazole and amide C=O. (C, G) NCI isosurface plot of **GH/Zn** and **AH/Zn** monomer, the isosurface is generated for s = 0.4 a.u. (D, H) One dimensional assembly of the **GH/Zn** (top) and **AH/Zn** (bottom) nanofibers through hydrogen bonding between the dimers. Note that, **GH/Zn** shows more twisted structure compared to **AH/Zn** due to the side chain adaptability of the glycine. Color code: C, gray; H, white; N, blue; O, red; Zn, steel blue.

Based on the analysis of various solvent systems as depicted in Figure 1B, we anticipate the H-bonds to be dynamic, with competition between the side chain and solvent interactions. To understand changes in H-bonding interactions, we studied GH/Zn and AH/Zn nanofibers using environmental Fourier transform infrared spectroscopy (FT-IR). FT-IR exhibited an intense peak at 1623 $cm^{-1}$ for GH/Zn (Figure S15), and AH/Zn gradually broadened upon hydration (Figure S16). For GH/Zn, we observed the greater broadening of 1623 $cm^{-1}$ peak at 70 % RH, while AH/Zn spectra did not show appreciable change.[53-55] The signal at 1455 $cm^{-1}$ due to carboxylate symmetric stretching also intensified with high RH. This finding led us to further explore the effects of RH on GH/Zn and AH/Zn nanofiber assemblies in the solid state. A customized RH-controlled AFM was employed to analyze changes in topography and mechanical properties. It was found that GH/Zn fibers fully disassembled at 60-70 % RH in a reversible manner, whereas AH/Zn nanofibers remained intact within the same RH (Figure 4A, and Video 1). The (dis-)assembly in the solid-state was further verified using environmental SEM and brightfield microscopy (Figure 4B and Figure S17-S19, and Video 2-3). AFM also revealed that GH/Zn reorganized into spherical structures upon hydration, where directional hydrogen bonding is displaced by interactions with water-vapor in line with FT-IR data (Figure S20).[53,55]

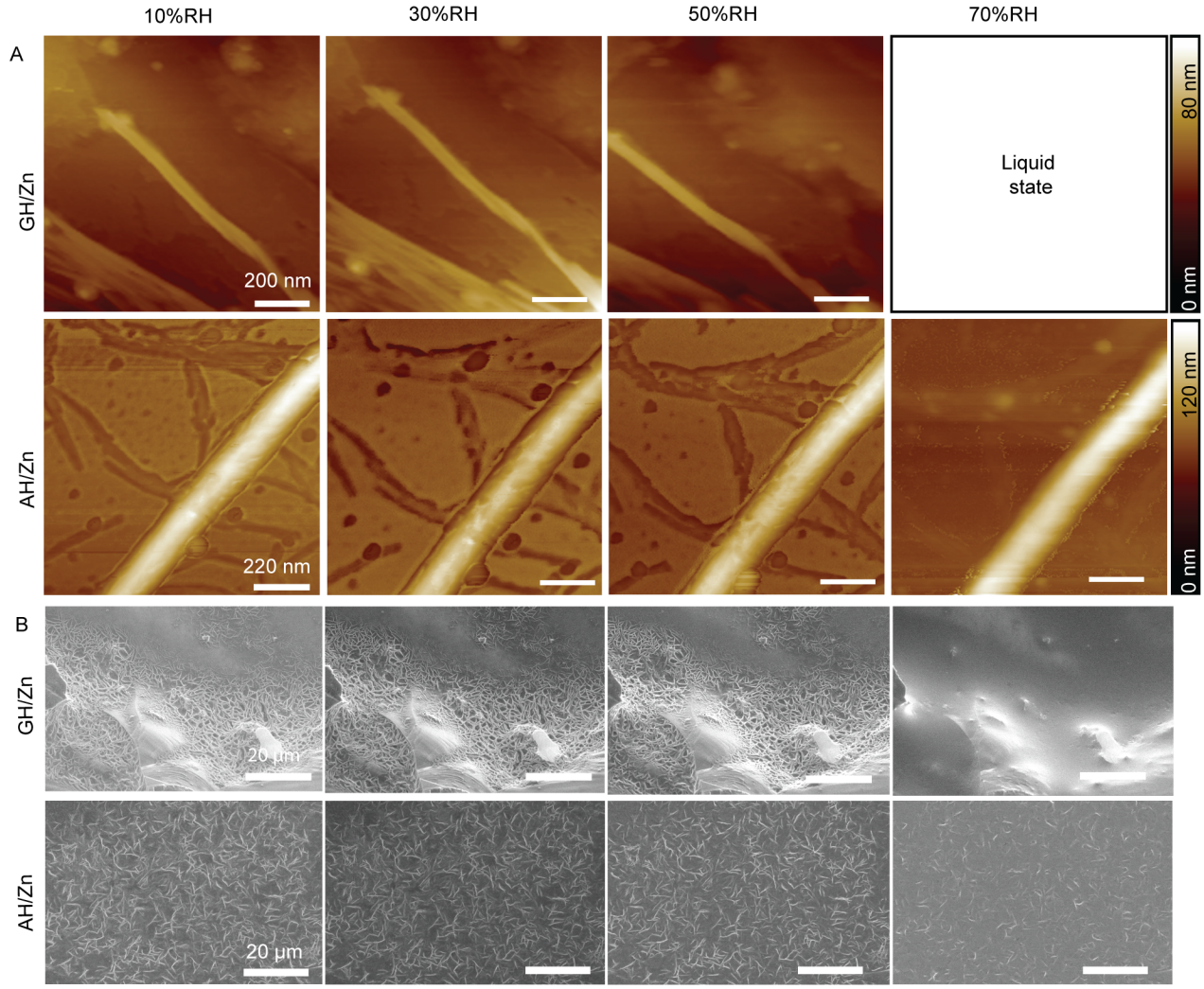


**Figure 4.** Vapor induced (dis)-assembly through varying RH. (A) Customized RH- dependent AFM topography shows the (dis)-assembly of the metallo-peptide nanofibers upon varying RH from 10 % and 70 %. (B) Environmental SEM shows morphologic changes of GH/Zn and AH/Zn nanofibers in response to RH change.

Using DFT calculations, we optimized water complexes featuring both GH/Zn and AH/Zn dimers, incorporating two water molecules inserted between the dimers which disrupt the intermolecular C=O···H–N hydrogen bonds (Figure S35 in SI). The energy of formation (ΔEw) for these complexes and their corresponding enthalpy change (ΔHw) are as follows: ΔEw values are -17.7 and -17.0 kcal/mol, while ΔHw values are -13.9 and -12.9 kcal/mol (details in SI, Table S5), respectively. The difference indicates the stability of both GH/Zn and AH/Zn dimers up to a certain point, but dissociation is more favorable in the case of GH/Zn dimer compared to the AH/Zn dimer.

To evaluate the water adsorption/desorption properties of the metallo-peptide nanofibers during humid/dry cycles, dynamic

vapor sorption (DVS) was performed. The water sorption isotherm revealed that GH/Zn had more tendency to adsorb water compared to the AH/Zn (Figure 5A). Specifically, the GH/Zn isotherm revealed a change in mass of 65 %, with a minimum water uptake between 5 % RH and 70 % RH; a step change was observed at 70 % RH correlating with the (dis-)assembly of the GH/Zn nanofibers at ~70 % RH in line with the FT-IR data (Figure 5A and Figure S15-S16). Whereas for AH/Zn, only a 30 % mass change was observed (Figure S21). Brunauer-Emmett-Teller (BET) analysis of the air-dried gels of GH/Zn and AH/Zn indicates the mesoporous nature of the bulk materials of the metallo-peptide nanofibers (Figure S22).

To understand the mechanical tunability of the metallo-peptide nanofibers with different RH, we performed nanoindentation to evaluate the Young's modulus using a RH-controlled customized AFM. A significant difference in the stiffness of GH/Zn and AH/Zn nanofibers was observed when RH was varied from ~10 % to 70 % (Figure 5B). GH/Zn nanofiber stiffness continuously decreased upon increasing RH, while AH/Zn shows a drop of the stiffness at 30 % RH which remains constant up to 70 % RH. This observation correlates with the (dis-)assembly of the GH/Zn leads to the gradual drop of the young moduli, while AH/Zn didn't lead to complete disassembly. Compared to previously reported hydrophobic core-based peptide nanofibers, both GH/Zn and AH/Zn nanofibers exhibited lower stiffness (1-4 GPa), which could be attributed to the coordination and solvation effects.[13-15,17] This observation indicates a correlation between the stiffness of GH/Zn and AH/Zn nanofibers with varying RH and also metallo-peptide-water-vapor interactions of GH/Zn and AH/Zn in the solid-state.

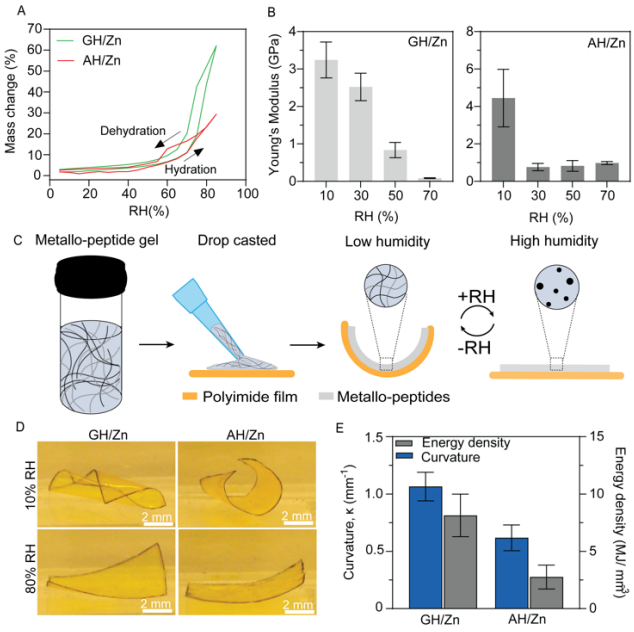


**Figure 5.** (A) Water sorption isotherms of the solid-state GH/Zn and AH/Zn nanofibers. (B) Young's moduli of water-vapor responsive stiffness changes for GH/Zn (left) and AH/Zn (right) nanofibers in the solid-state at different RH levels (10 % to 80 %). (C) Schematic representation of polar metallo-peptide nanofibers coated polyimide film responsible for water-vapor induced mechanical actuation properties. (D) Metallo-peptide nanofibers coated polyimide films reversibly folds/ unfolds in response to RH changes from 10- 80 % (scale bar, 2 mm). (E) Energy density of metallo-peptide nanofibers.

Finally, we investigated whether the supramolecular metallo-peptide-water-vapor interactions could be used to actuate a soft polymer film (Figure 5C). A polyimide film was coated with the metallopeptide nanofibers. Upon exposure to varying RH, both GH/Zn and AH/Zn coated polyimide film rapidly and reversibly curled and straightened over 50 cycles (Figure 5D, Figure S23 and video 4). The actuation energy density of GH/Zn and AH/Zn reaches 8.1 MJ/m$^3$ and 2.8 MJ/m$^3$, respectively (Figure 5E and Fig S23). These values are comparable with those of previously reported high-performance water-responsive peptide crystals.[15] The higher energy density of GH/Zn may be attributed to the relatively greater stiffness of GH/Zn across the entire RH range.

In summary, we introduce metallo-peptide nanofibers composed of hydrophilic dipeptides that coordinate Zn (II) ions and provide a polar interface. These nanofibers are produced by assembly and gelation in methanol/water at pH~12 followed by air drying. Notably, these nanofibers reversibly (dis-)assemble in the solid-state upon exposure to varying RH. Further, when metallo-peptide fibers were deposited onto polyimide films, the nanofibers exhibited rapid mechanical actuation and folding/unfolding of the polyimide film. The changes of the stiffness and morphology of the GH/Zn and AH/Zn demonstrated that peptide flexibility and hydrophilicity strongly influence the interactions between metallo-peptides and water vapor in the solid-state. We propose that the key driver is a rebalancing of H-bonding interactions between peptides and water, combined with the use of metal coordination. This work introduces design features for solid-state responsive peptide materials with tunable or erasable mechanical actuation properties triggered by water-vapor, which could be relevant for the developing responsive barrier materials and actuators.

## ASSOCIATED CONTENT

### Supporting Information

Methods and characterizations, materials, and synthetic procedures, supporting figures, supporting tables, and supporting references and movie.

## AUTHOR INFORMATION

### Present Addresses

[1]Nanoscience Initiative at Advanced Science Research Center of the Graduate Center of the City University of New York, New York, New York, 10031, USA.
[2]Department of Chemical Engineering, The City College of New York, 275 Convent Ave, New York, NY 10031, USA.
[3]Department of Chemistry, Cooch Behar Panchanan Barma University, Cooch Behar, West Bengal, 736101, India.
[4]Ph.D. Program in Physics, The Graduate Center of the City University of New York, 365 5th Ave, New York, NY 10016, USA.
[5]Department of Chemistry Hunter College, City University of New York, New York, New York, 10065, USA.
[6]Ph.D. Program in Chemistry, The Graduate Center of the City University of New York, 365 5th Ave, New York, NY 10016, USA.
[7]Ph.D. Program in Biochemistry, The Graduate Center of the City University of New York, 365 5th Ave, New York, NY 10016, USA.

### Funding Sources

RVU acknowledges funding from Office of Naval Research for the Vannevar Bush Faculty Fellowship (Grant No. N00014-21-1-2967). We thank the Air Force Office of Scientific Research for

funding of RVU, AD (Grant No. FA9550-23-1-0456). and the Army Research Office for funding of EN, RVU and X. C. (Grant No. W911NF-21-1-0172).

## ACKNOWLEDGMENT

RVU acknowledges funding from Office of Naval Research for the Vannevar Bush Faculty Fellowship (Grant No. N00014-21-1-2967). We thank the Air Force Office of Scientific Research for funding of RVU, AD (Grant No. FA9550-23-1-0456). and the Army Research Office for funding of EN, RVU and X. C. (Grant No. W911NF-21-1-0172). SZ, TL and MNN would like to acknowledge the Surface Science Facility at ASRC. RS acknowledges the Department of Science & Technology (DST), New Delhi, India for his DST-INSPIRE Faculty Fellowship (Faculty Registration No. IFA22-CH 378). RS is also thankful to C-DAC Patna, Meity, Government of India for the computational facility. We would like to acknowledge Vignesh Athiyarath for his assistance with the discussion and figure preparation.

## REFERENCES

1. Qing, R.; Hao, S.; Smorodina, E.; Jin, D.; Zalevsky, A.; Zhang, S. Protein Design: From the Aspect of Water Solubility and Stability. *Chem. Rev*. **2022**, *122*, 14085-14179.
2. Levin, A.; Hakala, T. A.; Schnaider, L.; Bernardes, G. J. L.; Gazit, E.; Knowles, T. P. J. Biomimetic peptide self-assembly for functional materials. *Nat Rev Chem* **2020**, *4*, 615-634.
3. Aida, T.; Meijer, E.W.; Stupp, S. Functional supramolecular polymers. *Science*, **2012**, *335(6070)*, 813-817.
4. Hamley, I. W. Self-assembly of amphiphilic peptides. *Soft Matter* **2011**, *7 (9)*, 4122-4138.
5. Yan, X.; Zhu, P.; Li, J. Self-assembly and application of diphenylalanine-based nanostructures. *Chem. Soc. Rev.* **2010**, *39*, 1877–1890.
6. Zhang, S. Fabrication of novel biomaterials through molecular self-assembly. *Nature Biotechnology* **2003**, *21(10)*, 1171-1178.
7. Sheehan, F.; Sementa, D.; Jain, A.; Kumar, M.; Tayarani-Najjaran, M.; Kroiss, D.; Ulijn, R. V. U. Peptide-Based Supramolecular Systems Chemistry. *Chem. Rev*. **2021**, *121*, 13869−13914.
8. Rabone, J.; Yue, Y. F.; Chong, S.; Stylianou, K.; Bacsa, J.; Bradshaw, D.; Darling, G.; Berry, N.; Khimyak, Y.; Ganin, A.; Wiper, P.; Claridge, J. B.; Rosseinsky, M. J. An Adaptable Peptide-Based Porous Material. *Science* **2010**, *329*, 1053– 1057.
9. Reches, M.; Gazit, E. Casting Metal Nanowires Within Discrete Self-Assembled Peptide Nanotubes. *Science* **2003**, *300*, 625– 627.
10. Shen, Y.; Levin, A.; Kamada, A.; Toprakcioglu, Z.; Rodriguez-Garcia, M.; Xu, Y.; Knowles, T. P. J. From Protein Building Blocks to Functional Materials. *ACS Nano* **2021**, *15*, 5819-5837.
11. Miserez, A.; Yu, J.; Mohammadi, P. Protein-Based Biological Materials: Molecular Design and Artificial Production. *Chem. Rev*. **2023**, *123*, 2049−2111.
12. Sahoo, J. K.; Hasturk, O.; Falcucci, T.; Kaplan, D. Silk chemistry and biomedical material designs. *Nat. Rev. Chem.* **2023**, *7*, 302-318.
13. Abramovich, L. A.; Kol, N.; Yanai, I.; Barlam, D.; Shneck, R.Z.; Gazit, E.; Rousso, I. Self-Assembled Organic Nanostructures with Metallic-Like Stiffness. *Angew. Chem*. **2010**, *122*, 10135 –10138.
14. F. K. Sheehan, H. Wang, D. Podbevšek, E. Naranjo, J. R.- Cancel, C. Moran, R. V. Ulijn, X. Chen, Aromatic Zipper Topology Dictates Water-Responsive Actuation in Phenylalanine-Based Crystals. *Small* **2023**, *19*, 2207773.
15. Piotrowska, R.; Hesketh, T.; Wang, H.; Martin, A. R. G.; Bowering, D.; Zhang, C.; Hu, C. T.; McPhee, S. A.; Wang, T.; Park, Y.; Singla, P.; McGlone, T.; Florence, A.; Tuttle, T.; Ulijn, R. V.; Chen, X. Mechanistic insights of evaporation-induced actuation in supramolecular crystals. *Nat. Mater*. **2021**, *20*, 403-409.
16. (a) Adams, D. J. Does Drying Affect Gel Networks? *Gels*, **2018**, *4(2)*, 32. (b) Dexter, A. F.; Malcolm, A. S.; Middelberg, A. P. J. Reversible active switching of the mechanical properties of a peptide film at a fluid-fluid interface. *Nat. Mater*. **2006**, *2*, 502-506.
17. Azuri, I.; Abramovich, L.A.; Gazit, E.; Hod, O.; Kronik, L. Why Are Diphenylalanine-Based Peptide Nanostructures so Rigid? Insights from First Principles Calculations. *J. Am. Chem. Soc*. **2014**, *136*, 963-969.
18. Wang, H.; Liu, Z.-L.; Lao, J.; Zhang, S.; Abzalimov, R.; Wang, T.; Chen, X. High Energy and Power Density Peptidoglycan Muscles through Super-Viscous Nanoconfined Water. *Adv. Sci.*, **2022**, *9*, 2104697.
19. Knowles, T. P. J.; Mezzenga, R. Amyloid Fibrils as Building Blocks for Natural and Artificial Functional Materials. *Adv. Mater*. **2016**, *28*, 6546-6561.
20. Dear, A. J.; Meisl, G.; Šariè, A.; Michaels, T. C. T.; Kjaergaard, M.; Linse, S.; Knowles, T. P. J. Identification of on- and off-pathway oligomers in amyloid fibril formation. *Chem. Sci*., **2020**, *11*, 6236–6247.
21. Wei, G.; Su, Z.; Reynolds, N.P.; Arosio, P.; Hamley, I.W.; Gazit, E.; Mezzenga, R. Self-assembling peptide and protein amyloids: from structure to tailored function in nanotechnology. *Chem. Soc. Rev*., **2017**, *46*, 4661-4708.
22. Bera, S.; Mondal, S.; Xue, B.; Shimon, L. J. W.; Cao, Y.; Gazit, E. Rigid helical-like assemblies from a self-aggregating tripeptide. *Nat. Mater.* **2019**, *18*, 503–509.
23. Panja, S.; Adams, D. J. Stimuli responsive dynamic transformations in supramolecular gels. *Chem. Soc. Rev.*, **2021**, *50*, 5165-5200.
24. Gazit, E. Self-assembled peptide nanostructures: the design of molecular building blocks and their technological utilization. *Chem. Soc. Rev*. **2007**, *36(8),* 1263-1269.
25. Levin, A.; Mason, T. O.; Abramovich, L. A.; Buell, A. K.; Meisl, G.; Galvagnion, C.; Bram, Y.; Stratford, S. A.; Dobson, C. M.; Knowles, T. P. J.; Gazit, E. Ostwald's rule of stages governs structural transitions and morphology of dipeptide supramolecular polymers. *Nat. Commun*. **2014**, *5*, 5219.
26. Wang, S.; Meng, X.; Zhou, H.; Liu, Y.; Secundo, F.; Liu, Y. Enzyme Stability and Activity in Non-Aqueous Reaction Systems: A Mini Review. *Catalysts* **2016**, *6*, 32.
27. Liu, X.; Zhu, P.; Fei, J.; Zhao, J.; Yan, X.; Li, J. Synthesis of Peptide-Based Hybrid Nanobelts with Enhanced Color Emission by Heat Treatment or Water Induction. *Chem. Eur. J.* **2015**, *21*, 9461–9467.
28. Chen, L.; Morris, K.; Laybourn, A.; Elias, D.; Hicks, M. R.; Rodger, A.; Serpell, L.; Adams, D. J. Self-Assembly Mechanism for a Naphthalene-Dipeptide Leading to Hydrogelation. *Langmuir* **2010**, *26*, 5232−5242.
29. Abramovich, L. A.; Aronov, D.; Beker, P.; Yevnin, M.; Stempler, S.; Buzhansky, L.; Rosenman, G.; Gazit, E. Self-assembled arrays of peptide nanotubes by vapour deposition. *Nat. Nanotech.* **2009**, *4,* 849-854.
30. Lampel, A.; Ulijn, R. V.; Tuttle, T. Guiding principles for peptide nanotechnology through directed discovery. *Chem. Soc. Rev*., **2018**, *47*, 3737-3758.
31. Bai, S.; Debnath, S.; Javid, N.; Frederix, P. W. J. M.; Fleming, S.; Pappas, C. G.; Ulijn, R. V. Differential Self-Assembly and Tunable Emission of Aromatic Peptide Bola-Amphiphiles Containing Perylene Bisimide in Polar Solvents Including Water. *Langmuir* **2014**, *30(25)*, 7576−7584.
32. Giudice, A.D.; Rüter, A.; Pavel, N.V.; Galantini, L.; Olsson, U. Self-Assembly of Model Amphiphilic Peptides in Nonaqueous Solvents: Changing the Driving Force for Aggregation Does Not Change the Fibril Structure. *Langmuir* **2020**, *36*, 8451−8460.
33. Jung, Y.; Khan, M. K.; Podbevšek, D.; Sudhakar, T.; Tu, R.S.; Chen, X. Enhanced water-responsive actuation of porous *Bombyx mori* silk. *Soft Matter* **2023**, *19*, 2047-2052.
34. Katsoulidis, A. P.; Antypov, D.; Whitehead, G. F. S.; Carrington, E. J.; Adams, D. J.; Berry, N. G.; Darling, G. R.; Dyer, M. S.; Rosseinsky, M. J. Chemical control of structure and guest uptake by a conformationally mobile porous material. *Nature* **2019**, *565*, 213–217.
35. Gastaldo, C. M.; Antypov, D.; Warren, J. E.; Briggs, M. E.; Chater, P. A.; Wiper, P. V.; Miller, G. J.; Khimyak, Y. Z.; Darling, G. R.; Berry, N. G.; Rosseinsky, M. J. Side-chain control of porosity closure in single- and multiple-peptide-based porous materials by cooperative folding. *Nature Chem* **2014**, *6*, 343–351.

36. Mabesoone, M. F. J.; Palmans, A. R. A.; Meijer, E. W. Solute–Solvent Interactions in Modern Physical Organic Chemistry: Supramolecular Polymers as a Muse. *J. Am. Chem. Soc.* **2020**, *142*, 19781–19798.
37. Weyandt, E.; Ter Huurne, G. M.; Vantomme, G.; Markvoort, A. J.; Palmans, A. R. A.; Meijer, E. W. Photodynamic Control of the Chain Length in Supramolecular Polymers: Switching an Intercalator into a Chain Capper. *J. Am. Chem. Soc.* **2020**, *142*, 6295–6303.
38. Pappas, C. G.; Shafi, R.; Sasselli, I. R.; Siccardi, H.; Wang, T.; Narang, V.; Abzalimov, R.; Wijerathne, N.; Ulijn, R. V. Dynamic peptide libraries for the discovery of supramolecular nanomaterials. *Nat. Nanotech*. **2016**, *11*, 960-967.
39. Omosun, T. O.; Hsieh, M.-C.; Childers, W. S.; Das, D.; Mehta, A. K.; Anthony, N. R.; Pan, T.; Grover, M. A.; Berland, K. M.; Lynn, D. G. Catalytic diversity in self-propagating peptide assemblies. *Nat. Chem*. **2017**, *9*, 805−809.
40. Fleming, S.; Ulijn, R. V. U. Design of nanostructures based on aromatic peptide amphiphiles. *Chem. Soc. Rev.,* **2014**, *43*, 8150-8177.
41. Draper, E. R.; Adams, D. J. Low-Molecular-Weight Gels: The State of the Art. *Chem* **2017**, *3(3)*, 390-410.
42. Lu, H.; Lutz, H.; Roeters, S.J.; Hood, M.A.; Schafer, A.; Muñoz-Espí, R.; Berger, R.; Bonn, M.; Weidner, T. Calcium-Induced Molecular Rearrangement of Peptide Folds Enables Biomineralization of Vaterite Calcium Carbonate. *J. Am. Chem. Soc*. **2018**, *140*, 2793-2796.
43. Boas, D.; Teijlingen, A. v.; Shpilt, Z.; Shalev, D. E.; Tshuva, E. Y.; Tuttle, T.; Reches, M. A multifunctional drug delivery system based on switchable peptide-stabilized emulsions. *Chem* **2024**, *10*, 1- 18.
44. Rufo, C. M.; Moroz, Y. S.; Moroz, O. V.; Stöhr, J.; Smith, T. A.; Hu, X.; DeGrado, W. F.; Korendovych, I. V. Short peptides self-assemble to produce catalytic amyloids. *Nature Chem* **2014**, *6*, 303-309.
45. Zhang, L.; Bailey, J. B.; Subramanian, R. H.; Groisman, A.; Tezcan, F. A. Hyperexpandable, self-healing macromolecular crystals with integrated polymer networks. *Nature*. **2018**, *557(7703*), 86-91.
46. Zhou, L.; Li, S.; Su, Y.; Yi, X.; Zheng, A.; Deng, F. Interaction between Histidine and Zn(II) Metal Ions over a Wide pH as Revealed by Solid-State NMR Spectroscopy and DFT Calculations. *J. Phys. Chem. B* **2013**, *117*, 8954- 8965.
47. Aduriz-Arrizabalaga, J.; Mercero, J. M.; Sancho, D.D.; Lopez, X. Rules governing metal coordination in Aβ–Zn(ii) complex models from quantum mechanical calculations. *Phys. Chem. Chem. Phys.* **2023**, *25*, 27618-27627.
48. Katsoulidis, A. P.; Park, K. S.; Antypov, D.; Marti-Gastaldo, C.; Miller, G. J.; Warren, J. E.; Robertson, C. M.; Blanc, F.; Darling, G. R.; Berry, N. G.; Purton, J. A.; Adams, D. J.; Rosseinsky, M. J. Guest-Adaptable and Water-Stable Peptide-Based Porous Materials by Imidazolate Side Chain Control. *Angew. Chem., Int. Ed*. **2014**, *53*, 193-198.
49. Y. Zhang, J. Wang, S. Zhao, M. Serdechnova, C. Blawert, H. Wang, M. L. Zheludkevich, F. Chen, Double-Ligand Strategy to Construct an Inhibitor-Loaded Zn-MOF and Its Corrosion Protection Ability for Aluminum Alloy 2A12. *ACS Appl. Mater. Interfaces* **2021**, 13, 51685−51694.
50. Stevens, J. S.; C. de Luca, A.; Pelendritis, M.; Terenghi, G.; Downes, S.; Sven L. M. Schroeder, S. L. M. Quantitative analysis of complex amino acids and RGD peptides by X-ray photoelectron spectroscopy (XPS). *Surf. Interface Anal*. **2013**, *45*, 1238–1246.
51. D. Iglesias, M. M.-Franco, M. Kurbasic, M. Melchionna, M. Abrami, M. Grassi, M. Prato, S. Marchesan, Oxidized Nanocarbons-Tripeptide Supramolecular Hydrogels: Shape Matters! *ACS Nano* **2018**, *12*, 5530- 5538.
52. Kim, J.; Park, K.; Cho, Y.; Shin, H.; Kim, S.; Char, K.; Choi, J. W. $Zn^{2+}$–Imidazole Coordination Crosslinks for Elastic Polymeric Binders in High-Capacity Silicon Electrodes. *Adv. Sci*. **2021**, *8*, 2004290.
53. Steinert, R. M.; Kasireddy, C.; Heikes, M. E.; Mitchell-Koch, K. R. Newly identified C–H···O hydrogen bond in histidine. *Phys. Chem. Chem. Phys*., **2022**, *24*, 19233-19251.
54. Baures, P. W.; Rush, J. R.; Wiznycia, A. V.; Desper, J.; Helfrich, B. A.; Beatty, A. M. Intramolecular Hydrogen Bonding and Intermolecular Dimerization in the Crystal Structures of Imidazole-4,5-dicarboxylic Acid Derivatives. *Cryst. Growth Des*. **2002**, *2(6)*, 653-664.
55. Scheiner, S.; Kar, T.; Pattanayak, J. Comparison of Various Types of Hydrogen Bonds Involving Aromatic Amino Acids. *J. Am. Chem. Soc*. **2002**, *124 (44)*, 13257-13264.